Interaction of Atomic and Molecular Hydrogen with Tholin Surfaces at Low Temperatures

Ling Li,[†] Hui Zhao,[†] Gianfranco Vidali,[†] Yechiel Frank,[‡] Ingo Lohmar,[‡] Hagai B. Perets,[¶] and Ofer Biham[*,‡]

Physics Department, Syracuse University, Syracuse, New York 13244, Racah Institute of Physics, The Hebrew University, Jerusalem 91904, Israel, and Harvard-Smithsonian Center for Astrophysics, Cambridge, Massachusetts 02138

E-mail: biham@phys.huji.ac.il

[*]To whom correspondence should be addressed
[†]Syracuse University
[‡]The Hebrew University
[¶]Harvard-Smithsonian Center

Abstract

We study the interaction of atomic and molecular hydrogen with a surface of tholin, a man-made polymer considered to be an analogue of aerosol particles present in Titan's atmosphere, using thermal programmed desorption at low temperatures below 30 K. The results are fitted and analyzed using a fine-grained rate equation model that describes the diffusion, reaction and desorption processes. We obtain the energy barriers for diffusion and desorption of atomic and molecular hydrogen. These barriers are found to be in the range of 30 to 60 meV, indicating that atom / molecule-surface interactions in this temperature range are dominated by weak adsorption forces. The implications of these results for the understanding of the atmospheric chemistry of Titan are discussed.

1 Introduction

In the last decade, the study of the interaction of hydrogen with surfaces at low temperatures has become a topic of interest in fields as different as hydrogen storage[1] and interstellar chemistry, where molecular hydrogen forms on the surfaces of dust grains.[2,3] In the latter field, there are several laboratories studying the mechanisms of reaction of molecular hydrogen in various space-like environments. Most laboratory research on the formation of molecular hydrogen on dust grain analogues, such as silicates,[4–6] amorphous carbon,[7] and ices,[8–10] has shown that this process proceeds by the Langmuir-Hinshelwood (LH) mechanism[11] and is governed by weak adsorption forces. In the case of formation of H_2 at higher temperatures (≈ 300 K), it was found[12] that D atoms sent onto a hydrogen-loaded amorphous carbon surface abstract H atoms to form HD. On tholins, an analogue of aerosol particles in Titan's atmosphere, it was claimed that at high temperatures (above 150 K) molecular hydrogen is formed via the Eley-Rideal (ER) abstraction mechanism.[13]

Titan's atmosphere is composed mostly of diatomic nitrogen ($> 95\%$) and methane.[14] The dissociation of methane and nitrogen in the upper atmosphere creates radicals that eventually aggregate in macroscopic particles that form the well-known brownish haze that surrounds Titan. Information on this haze is limited because of the difficulty of obtaining data from ground observatories or space

probes that would reveal its chemical structure.[15] Over the years, starting with the seminal work of Sagan and Khare,[16] analogues of those particles, called tholins, have been produced and characterized in many laboratories,[17–19] and they were found to reproduce the optical signature of Titan's haze. Although preparation methods vary, there has been a convergence about the basic properties of these analogues.[20] They have a general formula $C_xH_yN_z$ and consist of a disordered chain of highly unsaturated polymers. Functional groups have been identified.[20] For our investigation, we are interested in the addition or removal of hydrogen via the hydrogenation and abstraction of C−C and C−N double and triple bonds.[13]

The abundant presence of unsaturated hydrocarbons is an indirect verification of the lack of abundant atomic hydrogen in the stratosphere and mesosphere where a wealth of organics are detected.[21] To resolve this discrepancy, it was suggested that hydrogen, which is produced in the dissociation of CH_4, might recombine to form molecular hydrogen that then escapes into space.[22] The formation of molecular hydrogen in Titan's atmosphere follows the same constraints as the formation of H_2 in the interstellar medium.[23] The *binary* association of hydrogen atoms puts the protomolecule in a dissociated state that can make slow spin-forbidden transitions to the ground state, and the protomolecule promptly dissociates. It takes a third particle participating in the reaction to absorb the excess energy. In Titan's atmosphere, however, the density of hydrogen atoms and the total density are still too small (cf. Section 6) to allow a third atom to play this role. But formation of H_2 taking place *on the surface* of a third body can be efficient.[24] In the case of Titan, the third body is an aerosol particle. This view is, however, not universally shared. For example, a competing mechanism was proposed,[22] in which H_2 is catalyzed by C_4H_2 which is one of the most abundant hydrocarbon molecules in Titan's atmosphere. However, it was found that this scheme is inconsistent with other observations of abundance of C_2- and C_3- containing hydrocarbons.[21]

In a recent experiment,[13] the formation of HD molecules was studied by sending D atoms onto tholins. The desorption of the reaction product, HD, from the tholin surface was detected by a quadrupole mass spectrometer, while the change to the surface resulting from the interaction with D atoms was detected via infrared (IR) spectrometry in a separate experiment in another

apparatus. The sample temperature was in a range appropriate for actual aerosol particles, 160 K, but experiments were also performed at a higher temperature of 300 K.

The formation of HD was attributed to the Eley-Rideal reaction scheme, sometimes called "prompt reaction model"[25] in the astrophysics literature. In this model, the atom coming from the gas phase interacts directly with an atom on the surface without first becoming accommodated to it. Alternatively, the gas-phase particle might exchange only part of its energy and move at super-thermal energy across the surface. This is called the hot-atom mechanism.[26]

Most of the surface-catalyzed reactions known in the surface chemistry literature can be described by the familiar LH model. The ER reaction or the hot-atom mechanism have been positively identified only in the 1990's, and mostly on H-plated single crystal metal surfaces,[27,28] H-plated silicon,[29] H-plated graphite[30] and H-loaded amorphous carbon.[12] There are two major signatures to look for in order to identify the ER reaction model: the detection of super-thermal energy in the HD leaving the surface, and the time dependence of the HD yield during irradiation of the surface with D atoms. Such irradiation depletes the surface of H atoms by their reaction with incoming D atoms, and hence the measured HD yield decreases exponentially with the irradiation time.

When the tholin sample was first exposed to D atoms, a small increase in the HD signal was measured,[13] but there was little change in the HD signal over time. A similar observation was made for the formation of HD from the interaction of D with hydrogen-loaded amorphous carbon at room temperature.[12] In this experiment, the cross section for the reaction between an adsorbed H atom and an incoming D atom was obtained from IR data, and was found to be almost two orders of magnitude smaller than the one measured for the interaction of energetic H atoms on a graphite surface.[30] The weak time dependence of the HD signal was attributed to this very small value of the cross section.[12] Alternatively, we could interpret this result as caused by a small probability of reaction when a D atom hits an H atom that is on the surface.

In this paper we report on a study of the formation of molecular hydrogen (specifically, HD and D_2) on tholins at lower temperatures, below 30 K. At these low temperatures the diffusion and desorption processes are slower and the residence times of the weakly adsorbed atoms and

molecules on the surface are longer. This leads to reduced noise levels and enables us to determine whether the LH or the abstraction mechanism are operative. We obtain activation energies for the diffusion and desorption of hydrogen atoms (H and D without distinction) and molecules (HD and D_2) on or from the surface. To this end, we use thermal desorption spectroscopy coupled with an analysis using rate equation models. This work builds on methodologies developed in previous studies of the formation of molecular hydrogen on analogues of interstellar dust particles, such as silicates,[5,6,31] carbonaceous materials,[32] and ices.[8,33,34]

The Paper is organized as follows. In Section 2 we describe the experimental setup and the type of measurements performed. Section 3 presents the results of these measurements. We then explain in detail the rate equation model (Section 4) that we employ. The experimental data is analyzed using this model in Section 5, which contains our main results on the energy landscape. We discuss applications of our results in Section 6, before concluding with our Summary (Section 7).

2 Experimental Methods

2.1 Apparatus

The apparatus used for these experiments is the same as the one employed to study the formation of molecular hydrogen on interstellar dust grain analogues.[35] It consists of two atom beam lines and a sample / detector chamber. In the beam lines, hydrogen and deuterium gas is dissociated by two radio frequency sources. The beam in each line is formed in three differentially pumped stages and is highly collimated. A metrological laser coaxial with the line is used to align the beam such that the two beams strike the same spot on the sample. The partial pressure in the third stage is in the 10^{-8} Torr range, and this stage is separated from the ultra-high vacuum chamber by a 2.5 mm collimator. The main chamber has a base pressure in the low to mid 10^{-10} Torr range. The detector, a high performance Hiden triple pass quadrupole mass spectrometer, is mounted on a rotatable flange, and is configured so it can measure both the flux coming from the sample and the one from the beams; different masses can be probed simultaneously. The sample is mounted on a cold

finger, surrounded by a cold copper shield to improve cooling. In the experiments reported here, the cold finger was cooled with liquid helium and the desired sample temperature was obtained using a cartridge heater (Lakeshore). The temperature was measured with a calibrated silicon diode (Lakeshore).

We use beam lines since they allow to control the kinematic conditions of irradiation of the sample to very good extent. Through differential pumping and the use of a mechanical chopper, low doses of H and D can be sent. Although the flux is understandably orders of magnitude higher than in actual space conditions, it is much less than traditionally achieved in laboratory experiments (cf. Sections 2.2 and 6). The reason for having two lines is that even if we use a very effective dissociation source ($\approx 75\%$), a small fraction of D_2 is transmitted on towards the sample. Deuterium is used instead of hydrogen because it is easier to detect HD as the product of reaction than H_2, which is the main residual gas in a well-baked ultra-high vacuum stainless steel chamber.

Additionally, the apparatus was instrumented with an IR spectrometer (Nicolet FT-IR 6300) in the reflection-absorption infrared spectroscopy (RAIRS) configuration in order to study in-situ surface modifications. The IR light from the source is sent into the apparatus via a differentially pumped MgF window. The beam strikes the sample at glancing incidence ($\approx 84^\circ$) and is then collected by a liquid nitrogen cooled mercury cadmium telluride detector placed outside the vacuum chamber. This arrangement grants high sensitivity and allows to perform the IR measurements without breaking the vacuum.

The sample was prepared by Prof. Mark Smith's laboratory (University of Arizona). The tholin films were deposited on a gold plated copper disc of $1/2$ inch diameter and 1 mm thickness. The films are thick (> 500 nm) and were produced over 4 days in a 10 kV AC discharge in 2% Methane and 98% N_2 at 14 Torr and at 300 K. Preparation and characterization methods of tholins made by arc discharge—as the ones used here—have been described before.[36,37] This preparation method yields tholins that are similar but not identical to the ones prepared at lower pressure. However, the higher pressure is necessary to obtain a film thick enough for use in these experiments. More details and comparisons can be found in the recent literature.[15,20,36,37] Characterization using Fourier-

transform ion cyclotron mass spectrometry is available as well.[38] A Fourier transform infrared (FTIR) spectrum of the sample prior to exposure to hydrogen is shown in Figure 1.

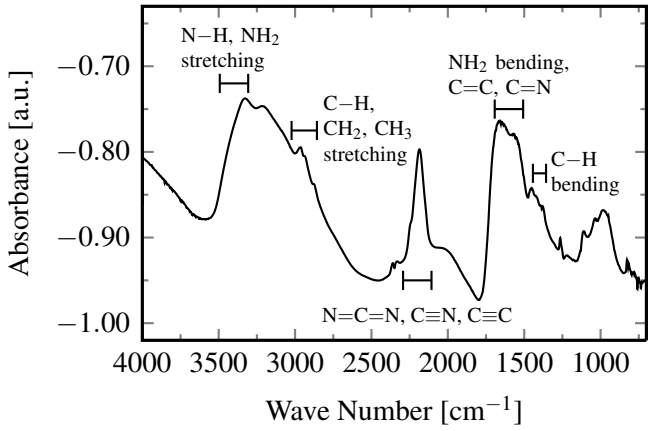

Figure 1: RAIRS spectrum of the tholin sample prior to exposure to hydrogen and deuterium atoms. Characteristic bands are shown.

Each sample was sent in a sealed pouch and was mounted on the sample holder while working under a flow of dry nitrogen. The vacuum chamber was pressurized with dry nitrogen gas before the insertion of the sample holder. Several samples were used in the experiments; for cleaning purposes, while in vacuum, the samples were taken to 350 K. One of them was also analyzed using an Atomic Force Microscope (AFM) (KLA-Tecnor P16+). Figure 2 shows that on a 2 μm linear scale, there is a height-to-height variation of 100 nm.

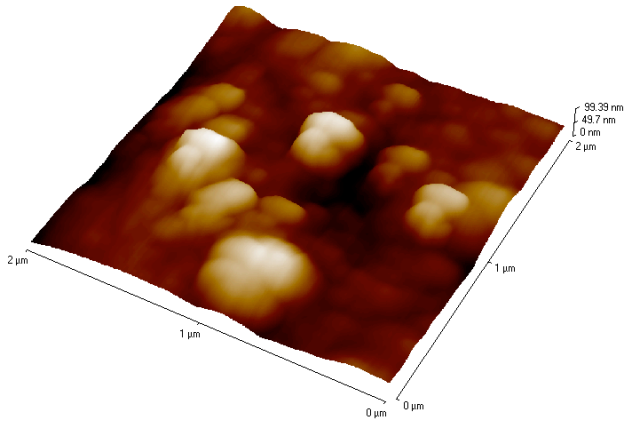

Figure 2: Three-dimensional rendering of an AFM scan on a tholin sample. The area covered is 4 μm^2 and the maximum height variation over this area is 100 nm.

2.2 Experimental Procedures

In temperature programmed desorption (TPD) experiments, the surface is first exposed to beams of atoms or molecules, at a fixed sample temperature and for a set amount of time. The sample temperature is then ramped up and the products desorbing from the surface are detected in real time. In the experiments presented here, we start the heating at a rate of about 6 K/s that decreases to 0.06 K/s eventually. During the experiment the amount dN of gas particles detected within a small (and constant) time interval dt is recorded. Simultaneously, we measure the sample temperature $T(t)$ (see Figure 3 for an example). To be able to compare several desorption measurements, we need to convert the rate dN/dt to the detection "rate" dN/dT with respect to temperature T. In practice, we first fit a function $T(t) = \text{const} \cdot t^{\gamma}$ to the temperature ramp ($t = 0$ corresponds to the start of heating). From this we determine dT/dt, unaffected by noise in the original measurement. We then obtain

$$\frac{\mathrm{d}N}{\mathrm{d}T}(T) = \frac{\mathrm{d}t}{\mathrm{d}T} \cdot \frac{\mathrm{d}N}{\mathrm{d}t}(t). \tag{1}$$

In the rate equation simulation we use a similar procedure. After every time step of the Runge-Kutta procedure we calculate the temperature change during that step, according to the fit for $T(t)$. From this we directly obtain the value of dN/dT in the simulation.

The shape and the position of peaks in d$N(T)$/dT provide information on the kinetics and energetics of the reactions, as illustrated below. In the experiment performed using simultaneous H and D beams, one probes the amount of HD formed on the surface. HD can form on the surface either rapidly (compared to laboratory time scales) due to fast diffusion, essentially while the sample is still being irradiated with H and D, or it can form during the heat pulse when the H and D atoms that became adsorbed on the surface during the irradiation phase become mobile, encounter each other and form HD.

The fluxes of the beams are measured using the rotatable quadrupole mass spectrometer without exposing the samples to the beams. The detector is placed between the beam lines (which are 38° apart) and the signals are recorded in real time. The measured effective beam density reaching the

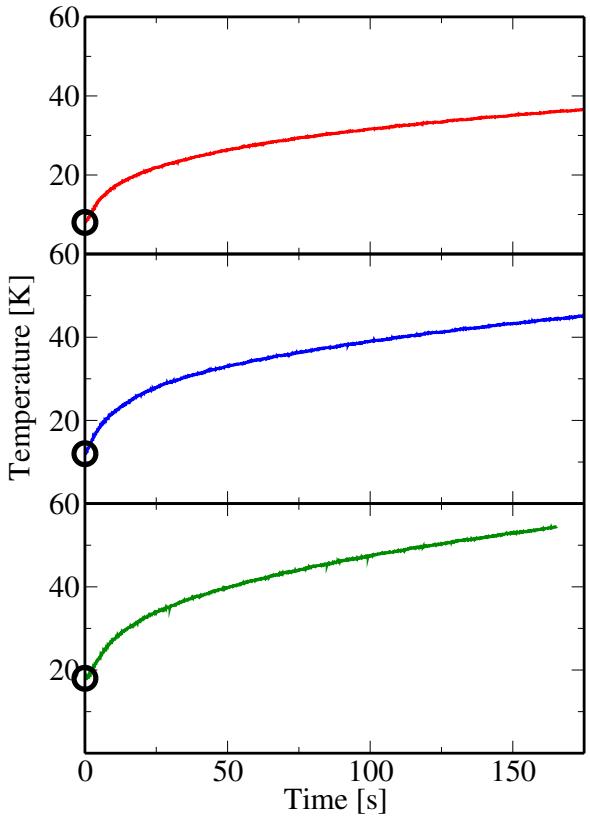

Figure 3: Temperature ramp of the sample for different irradiation temperatures: 8 K (top), 12 K (middle) and 18 K (bottom). These curves as measured in the experiment with irradiation of HD molecules. The irradiation temperature is marked by the circle on the temperature axis.

surface (after chopping) is $f_b = 5 \times 10^{10}$ cm^{-2} s^{-1}. The effective flux to the surface is estimated as follows. We assume a density $s \approx 5 \times 10^{14}$ sites/cm^2 of adsorption sites on the tholin surface. This is a reasonable value based on data for other materials such as silicates.[5] We thus obtain an effective flux of $f = f_b/s = 1 \times 10^{-4}$ monolayers (ML)/s.

3 Experimental Results

3.1 Eley-Rideal Prompt Reaction

In the "prompt reaction" scheme, a D atom abstracts a hydrogen atom on the surface, forming an HD molecule which leaves the surface. Such reaction has been observed in H-plated metals and graphite and on H-loaded amorphous carbon. The typical cross section is expected to be of the order of a few Å^2.[28–30] However, as already mentioned in the Introduction, a much smaller value of $\sim 3 \times 10^{-2}$ Å^2 was found on H-loaded amorphous carbon.[12] During the irradiation phase, the detector is positioned to measure any HD coming off the surface. For irradiation of H and D on tholin samples at low temperature, we find this contribution indistinguishable from the background. We thus conclude that the prompt reaction mechanism is inefficient under the physical conditions used here.

3.2 Langmuir-Hinshelwood Reaction

These experiments are similar in methodology to the ones we carried out on interstellar dust grain analogues.[6,35] In Figure 4 we present the desorption rate of HD molecules vs. temperature, after irradiation of HD molecules on the surface at surface temperatures of 8 K, 12 K and 18 K. The irradiation time was 120 s at 8 K, while for the higher temperatures the sample was irradiated for 240 s. The peak positions of a trace can be related to the activation energy of desorption.[39] The trace obtained after irradiation at 8 K consists of two peaks—a large peak at low temperature and a small peak at a somewhat higher temperature. This indicates that there are at least two types of

adsorption sites for HD molecules on the tholin surface. The relative areas below the two peaks suggest that there is a large number of shallow binding sites and a much smaller number of deep binding sites. The trace obtained after irradiation at 12 K exhibits a similar shape; however, its peak heights are decreased and its low-temperature edge is shifted to higher temperatures. This can be explained by the fact that at a surface temperature of 12 K those molecules adsorbed in shallow sites may quickly desorb already during irradiation. This effect is even more pronounced in the case of irradiation at 18 K, where the low-temperature peak has completely vanished.

A similar set of TPD traces for D_2 molecules is shown in Figure 5. Irradiation temperatures and times are as for the HD case. Everything we said about the traces for HD molecules applies here as well, but the peaks of traces of D_2 desorption are shifted to higher temperature with respect to the peaks of HD. This is due to the isotope effect. If we take the trapping potential to be a harmonic oscillator with an (unknown) "spring" constant k, then the lowest energy level for a molecule of mass m in this potential is $\hbar\sqrt{k/m}/2$. The higher atomic mass of D_2 molecules therefore leads to a lower ground state energy, which in turn leads to a larger activation energy for desorption.

As previously found in the analysis of HD and D_2 formation on amorphous silicates at different temperatures,[6] there is a common trailing edge in the three traces. This corroborates our fundamental assumption that the frequency and magnitude of certain energy barriers are properties of the surface morphology, and as such do not depend on the surface temperature during irradiation. An analysis of the shapes of these traces provides information on the distribution of binding energies, as we will show below.

Figures 6 and 7 show TPD curves after irradiation with H and D *atoms* and detecting HD, and with only D *atoms* and detecting D_2, respectively. The irradiation time is 120 s throughout, and irradiation temperatures are 8 K, 12 K and 22 K. In both cases, for HD as well as for D_2 detection, we observe that the traces have shapes very similar to their corresponding counterpart obtained from irradiation with molecules (Figures 4 and 5). Depending on the irradiation temperature, however, peaks of the TPD curves obtained by the association of atoms are shifted to higher temperatures relative to the ones obtained after irradiation with molecules. We observe this shift for both HD and

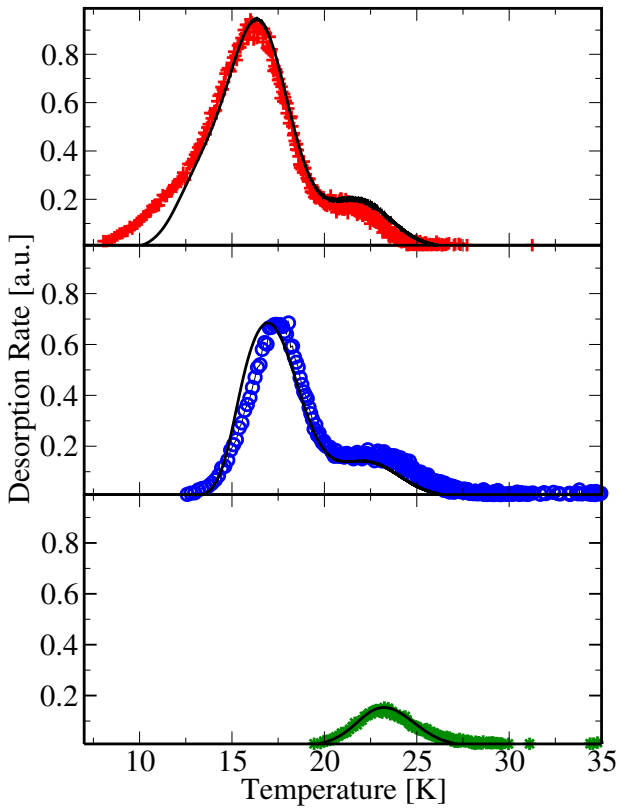

Figure 4: Desorption rate of HD molecules vs. temperature after irradiation of the surface with HD molecules. Irradiation temperatures 8 K (top), 12 K (middle) and 18 K (bottom). Colored symbols: Experimental data. Black lines: Fit using the rate equations (reduced model).

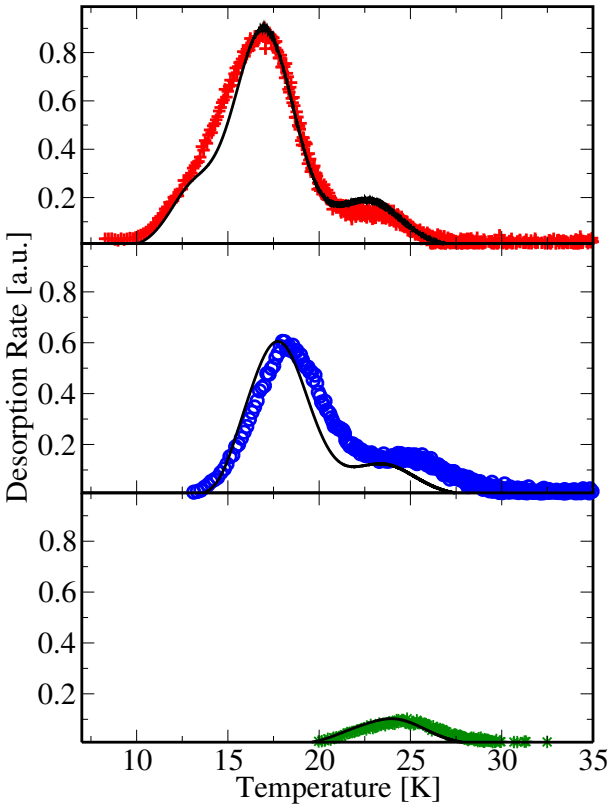

Figure 5: Desorption rate of D_2 molecules vs. temperature after irradiation of the surface with D_2 molecules. Irradiation temperatures and symbols as in Figure 4.

D_2 formation for the intermediate irradiation temperature of 12 K. We cannot explain this feature easily, and will return to this in our analysis in Section 5. For the case of HD, a comparison between molecule and atomic irradiation is shown in Figure 8. Note that the shift between the bottom panels of Figures 4 and 6, and of Figures 5 and 7, respectively, first and foremost reflects the fact that atomic irradiation was done at 22 K, while molecular irradiation was done at 18 K. Performing both types of experiment after irradiation at 18 K, we still found a shift (not shown), but of significantly smaller size ($\approx$ 1 K) than for the comparison at 12 K.

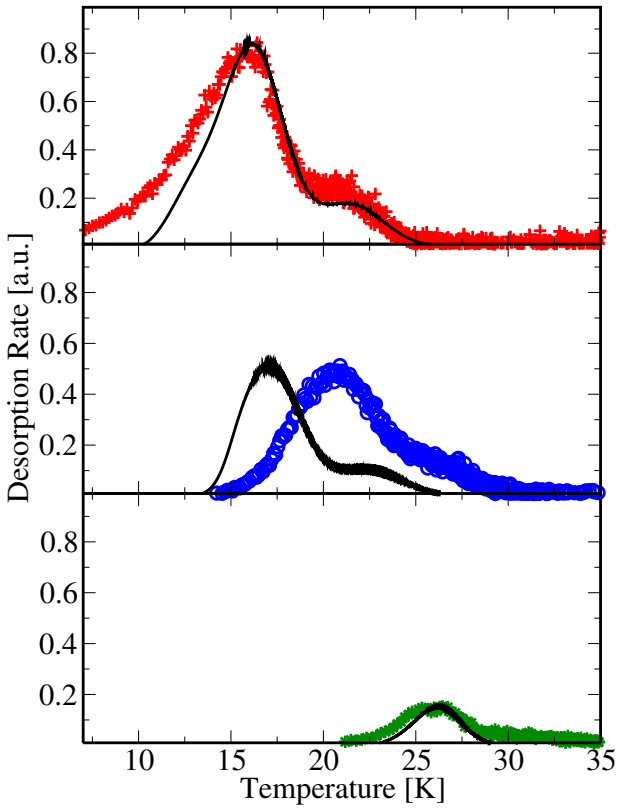

Figure 6: Desorption rate of HD molecules vs. sample temperature after irradiation of the surface with H and D atoms. Irradiation temperatures 8 K (top), 12 K (middle) and 22 K (bottom). Colored symbols: Experimental data. Black lines: Fit using the rate equations (reduced model).

The diminishing intensity of the signal with increasing irradiation temperature indicates that the processes involved in the formation of HD from H and D atoms are governed by weak physical adsorption forces, implying lower sticking probability of H and D at higher sample temperature. The widths of the traces are larger than the ones expected if there were only a single activation

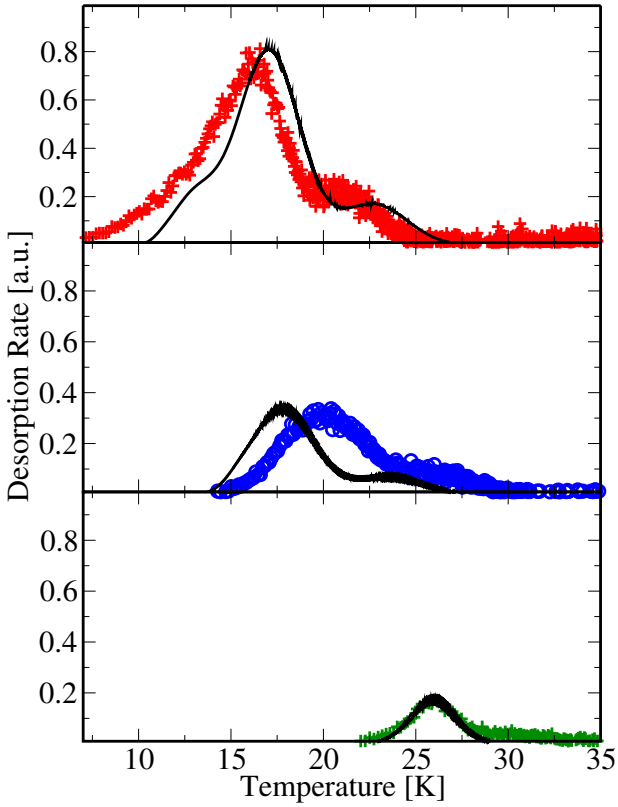

Figure 7: Desorption rate of D_2 molecules vs. sample temperature after irradiation of the surface with D atoms. Irradiation temperatures and symbols as in Figure 6.

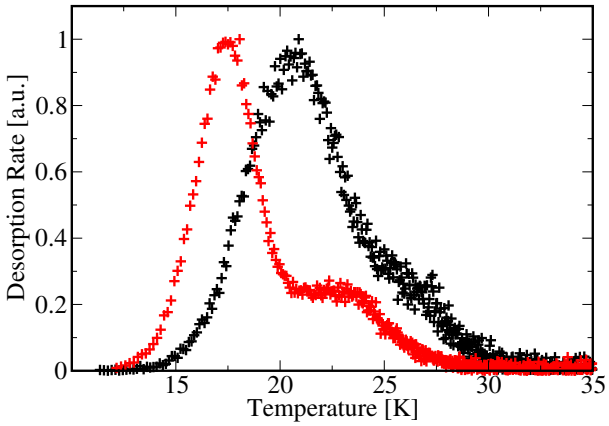

Figure 8: Comparison of the desorption rate of HD molecules vs. sample temperature, after irradiation of the surface with HD molecules (red pluses) and after irradiation with H and D atoms (black pluses), both at 12 K. The traces are normalized.

energy for desorption. Rather, similarly to what we detected in the formation of HD on amorphous silicates[6] but to a lesser degree, there is a range of activation energies.

We further note that the trailing edges of traces obtained after irradiation at different temperatures do *not* coincide for atomic irradiation, in contrast to what we found for molecular irradiation. This implies that the process of molecular formation (whether during irradiation or during the subsequent heating) affects the distribution of molecules to the different types of adsorption sites, in a way that depends on the surface temperature.

4 Rate Equation Model

In all TPD curves considered here we observe that most of the hydrogen is desorbed well before 40 K. We therefore conclude that the particles are trapped in physisorption potentials and are only weakly adsorbed. We also assume that the mechanism of formation of H_2 (or HD or D_2) is the LH scheme, as there is no evidence of prompt reaction.

The analysis of TPD experiments usually starts with the Polanyi-Wigner expression for the desorption rate,

$$R(t) = \nu N(t)^{\beta} \exp\left(\frac{-E}{k_{\mathrm{B}}T}\right). \tag{2}$$

In this expression, $N(t)$ is the total number of atoms on the surface, β is the order of desorption, and ν is the vibration frequency of the particle in the potential well where it is bound, also referred to as the attempt frequency. The effective activation energy is denoted by E, and $T = T(t)$ is the time-dependent surface temperature. One important assumption we make here is that all the surface properties, such as the attempt frequency and the energy barriers, are independent of temperature and population. This assumption is justified due to the low coverage of the surfaces during a TPD experiment (< 0.01 ML), but it might be violated at high coverages.[40] Analyses of TPD experiments using rate equations have been reported previously.[32,34,41] Here we introduce two models for describing the TPD experiments (for molecule as well as for atomic irradiation), a complete model accounting for all possible processes in the system, and a reduced one. We show

that the reduced model gives good results in fitting the experimental data.

4.1 Complete Model for Irradiation with Molecules

We first introduce the model for molecules only. It will be modified below to deal with atoms and their reactions. Molecules of a given species are sent onto the surface, and if they impinge onto an empty adsorption site, they stick to it with a certain probability. The rate at which particles stick to the (empty) surface is the *effective* flux f (in ML/s). Afterwards they may hop from a site to any of the neighboring sites, and may also desorb. Throughout we assume the rates for both processes to be thermally activated, with a common fixed attempt frequency ν (taken standardly to be 10^{12} s^{-1}). The hopping rate is given by

$$D = \nu \exp\left(\frac{-E^{\mathrm{diff}}}{k_{\mathrm{B}}T}\right), \tag{3}$$

where E^{diff} is the activation energy for diffusion, and $T(t)$ is the time-dependent temperature of the surface during the TPD experiment. The activation energy in general depends on the particle species and the type of site it is located at, both of which will later appear as indices on E^{diff} as well as on D. Similarly, the desorption rate reads

$$W = \nu \exp\left(\frac{-E^{\mathrm{des}}}{k_{\mathrm{B}}T}\right), \tag{4}$$

where E^{des} is the activation energy for desorption, which can also depend on the site type and the species. As the surface temperature increases, both the hopping rate and the desorption rate rapidly increase.

We now make several assumptions. First, we assume a given density of adsorption sites on the surface, each containing at most one molecule. We recognize that for the diffusion and desorption of H_2 (HD and D_2) molecules the surface is not homogeneous. We model this by using several types of sites, distinguished by *Greek* indices in our notation. Each type α has its own *average* energy barrier for diffusion, E_α^{diff}, and for desorption, E_α^{des}. Additionally, the energies for specific sites of type α are distributed according to a normal distribution around the average energy. The

standard deviation of this normal distribution is labeled σ_α. In order to retain detailed balance we set $E_\alpha^{\mathrm{des}} = E_\alpha^{\mathrm{diff}} + \Delta E$, where ΔE is an overall constant. An analogous relation holds for the desorption and diffusion barrier of each individual site, hence both energy distributions have the same standard deviation σ_α. Each type α of sites constitutes a fraction ρ_α of the entire surface such that $\sum_\alpha \rho_\alpha = 1$.

In a rate equation model, we cannot employ a continuous distribution of energies, and neither can we model a particular realization of surface site energies. (Note that a continuous distribution of binding energies can be obtained by direct inversion of TPD traces,[10,42,43] but this method does not include the possibility of simultaneous recombination processes.) We approximate the distribution of binding energies of a certain site type α around the mean value by using 21 different binding energies as samples for each type. The energy values are equidistantly spaced between $E_\alpha^{\mathrm{des}} - 3\sigma_\alpha$ and $E_\alpha^{\mathrm{des}} + 3\sigma_\alpha$. The fraction of sites at any given sample energy is chosen proportional to the value of the normal probability distribution function with mean E_α^{des} and standard deviation σ_α at that energy. This sampling of energies is schematically depicted in Figure 9. The individual sample will

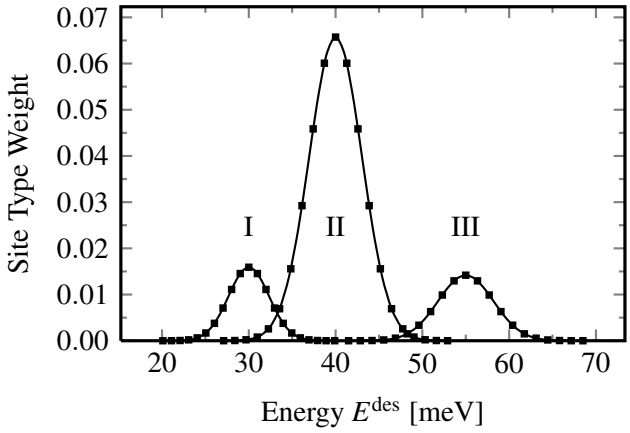

Figure 9: A schematic picture of the sampling of energies to model the normal distribution around mean energies, for three types of sites. The three normal distributions of binding energies for site types I, II, and III, respectively (solid lines), and the 21 sample energies used to model each distribution (black squares) are shown. Mean values and widths are taken from the results we obtain for HD molecules (see Section 5).

be denoted by a Latin index, e.g., E_i^{des}, and the weights of sites of the 21 sample energies add up to the total fraction of the 'fundamental' site type, $\rho_\alpha = \sum_{i \in \mathrm{type}\ \alpha} \rho_i$, hence $\sum_i \rho_i = 1$ again. For the

rate equation model, we effectively just have a large number of different site types, and we do not need to distinguish what basic type of site α they belong to. Hence, we shall still speak of different 'types' of sites also for the different i.

Let n be the coverage of molecules on the surface (in ML) and n_j that part of the total surface coverage which is trapped in sites of type j. Then $n_j \leq \rho_j$ and $n = \sum_j n_j \leq 1$. The set of rate equations for our model reads

$$\begin{aligned} \frac{\mathrm{d}n_i}{\mathrm{d}t} &= f(\rho_i - n_i) + \sum_{j \neq i} D_j n_j (\rho_i - n_i) \\ &\quad - D_i n_i \sum_{j \neq i} (\rho_j - n_j) - W_i n_i. \end{aligned} \tag{5}$$

The first term on the right hand side of Eq. (5) covers the incoming flux of molecules. The value of the effective flux f is found as described in Section 2.2. This term also accounts for LH rejection, such that all molecules impinging on top of a site already occupied are rejected. The second term describes the diffusion of molecules, arriving *from* other sites j. Likewise, the third term is the loss of molecules by diffusion from sites of type i to sites of any other type j. The hopping rate D_j on sites of type j is determined by the activation energy for diffusion on such sites, E_j^{diff}. The last term models desorption of molecules, with a desorption rate W_i determined by E_i^{des}, the activation energy for desorption from a site of type i. The rate at which molecules are detected during the experiment is therefore proportional to the total desorption rate

$$R = \sum_i W_i n_i. \tag{6}$$

This model accounts for all possible processes of motion of molecules: molecules can diffuse from any site type to any other site type and they can desorb.

To obtain the energy barriers for molecule diffusion and desorption, we examined the TPD curves of experiments in which molecular HD or D_2 were deposited on the surface during the irradiation phase and were later desorbed from the surface as the temperature increased (see Figures 4 and 5).

These curves show a broad distribution of temperatures at which molecules desorb from the surface, and two or three desorption peaks within this range. We therefore use three average activation energy barriers, each with an additional normal distribution of the energy (totaling 63 sample energies E_i). The fraction ρ_α (of sites of type α) found here is kept constant for all fits and experiments, see Section 5 for the results.

4.2 Complete Model for Irradiation with Atoms

We will now modify the model to describe the following situation. H atoms (precisely, H and D, or only D) are sent onto the surface and stick to empty sites with a certain effective flux. Atoms explore the surface just like molecules, and they can desorb as well. Additionally, when two atoms meet, they form a molecule.

To keep the number of parameters small, we do not distinguish between H and D atoms in our model, both species implicitly sharing the activation energies for desorption and diffusion. Experimentally, however, the isotope effect is observed and yields different energies for H+D vs. D+D experiments. The implications of this approximation have been examined.[31] The activation energies of desorption and diffusion of D atoms were raised by about 10% (this is comparable to the isotope effect measured in H and D scattering experiments from a graphite surface[44]). The TPD traces hardly changed because they mainly depend on the energetics of the most mobile species.

All assumptions detailed in the molecule model will remain in effect, including the uniform standard attempt frequency. Each adsorption site can now hold either an H or a D atom, or an HD or D_2 molecule. To simplify equations we assume that molecules and atoms on the surface do not encounter each other while hopping; this is justified due to the low coverage during TPD experiments. In contrast to the situation for molecules, we further assume that all sites are identical both for hopping and desorbing of atoms, hence the energy barriers $E_{\mathrm{H}}^{\mathrm{des}}$ and $E_{\mathrm{H}}^{\mathrm{diff}}$ are uniform all over the surface. Here and in the following, all quantities will get an extra index for the atom or molecule species. However, by our above comment, we do not distinguish between H and D, so that all atoms are labeled H, and all molecules H_2.

We denote by n_{H} the coverage of H atoms on the surface (in ML) and by $n_{\mathrm{H}_2,j}$ that part of the total surface coverage of H_2 molecules (in ML) which is trapped in sites of type j. Consequently, $n_{\mathrm{H}_2,j} \leq \rho_j$ and $n_{\mathrm{H}} \leq 1$. The new set of rate equations is now given by

$$\frac{\mathrm{d}n_{\mathrm{H}}}{\mathrm{d}t} = f(1-n_{\mathrm{H}}) - W_{\mathrm{H}} n_{\mathrm{H}} - 2D_{\mathrm{H}} n_{\mathrm{H}}^2, \tag{7a}$$

$$\begin{aligned}\frac{\mathrm{d}n_{\mathrm{H}_2,i}}{\mathrm{d}t} = {} & \frac{\rho_i - n_{\mathrm{H}_2,i}}{\sum_j (\rho_j - n_{\mathrm{H}_2,j})} D_{\mathrm{H}} n_{\mathrm{H}}^2 \\ & + \sum_{j \neq i} D_{\mathrm{H}_2,j} n_{\mathrm{H}_2,j} (\rho_i - n_{\mathrm{H}_2,i}) \\ & - D_{\mathrm{H}_2,i} n_{\mathrm{H}_2,i} \sum_{j \neq i} (\rho_j - n_{\mathrm{H}_2,j}) - W_{\mathrm{H}_2,i} n_{\mathrm{H}_2,i}.\end{aligned} \tag{7b}$$

The first term on the right hand side of Eq. (7a) describes the incoming flux of *atoms*, including LH rejection. f is the *effective* flux as explained before, only for atoms. The second term describes the desorption of atoms. The desorption rate W_{H} is governed by $E_{\mathrm{H}}^{\mathrm{des}}$ as specified above. The last term in Eq. (7a) is the recombination term, i.e., the rate of molecule formation on the surface. Here the hopping rate D_{H} is determined by $E_{\mathrm{H}}^{\mathrm{diff}}$. Eq. (7b) is the set of equations describing the dynamics of the molecules on the surface. The first term in Eq. (7b) consists of two factors. The second factor, $D_{\mathrm{H}} n_{\mathrm{H}}^2$ is the rate of molecule production as given by Eq. (7a); we assume that all molecules remain on the surface once they are formed, as observed experimentally. The first factor of this term distributes the molecules between the different types of sites according to the distribution of *free* sites among them. The remaining terms of Eq. (7b) have been explained above in the molecular model. The only difference is in the notation, since all quantities now carry the additional species label.

4.3 Reduced Models

The complete model for irradiation with molecules successfully fits the TPD experiments (not shown), but the best fits are obtained for energy barriers for the diffusion of molecules which are much *larger* than the barriers for desorption. This means that the process of molecular diffusion on

the surface can be neglected in *all* models.

Neglecting the two corresponding terms (diffusion of molecules to and from sites of type i) in the model of molecules only, Eq. (5), we obtain the simple model

$$\frac{\mathrm{d}n_i}{\mathrm{d}t} = f(\rho_i - n_i) - W_i n_i. \tag{8}$$

For irradiation with atoms instead, Eqs. (7), the reduced model takes the form

$$\frac{\mathrm{d}n_\mathrm{H}}{\mathrm{d}t} = f(1 - n_\mathrm{H}) - W_\mathrm{H} n_\mathrm{H} - 2D_\mathrm{H} n_\mathrm{H}^2, \tag{9a}$$

$$\frac{\mathrm{d}n_{\mathrm{H}_2,i}}{\mathrm{d}t} = \frac{\rho_i - n_{\mathrm{H}_2,i}}{\sum_j (\rho_j - n_{\mathrm{H}_2,j})} D_\mathrm{H} n_\mathrm{H}^2 - W_{\mathrm{H}_2,i} n_{\mathrm{H}_2,i}. \tag{9b}$$

As we show in the next section, these reduced models provide good fits to the experimental data. We use these models to obtain our results on activation energies and to produce the fits seen in Figures 4 to 7.

5 Analysis of Experimental Data

We now use the rate equations presented above to obtain the parameters that describe the dynamics of atoms and molecules on the tholin surface. The appropriate set of rate equations, i.e., Eqs. (5), (7), (8) or (9), respectively, is numerically integrated using a Runge-Kutta stepper. The result of that integration is a TPD curve that is then compared with the experimental one. The parameters are iteratively adjusted to obtain the best agreement.

5.1 Irradiation with Molecules

The TPD curves of HD and D_2 molecules (Figures 4 and 5) on tholin surfaces show a very broad distribution with two distinctive peaks, or one large peak and a shoulder at higher temperatures. The large low-temperature peak is most accurately described as two overlapping peaks, so that the entire curve is best described assuming desorption of molecules from three different types of sites, each

with normally-distributed activation energies.

The fitting curves for HD and D_2 irradiation at surface temperatures of 8 K, 12 K and 18 K are presented in Figures 4 and 5. The activation energies we find for desorption of molecules are given in Table 1. Recall that diffusion of molecules has been found to be negligible in our fitting procedure.

Table 1: Surface Parameters Obtained by Fitting Rate Equation Solutions to TPD Curves

	Fraction of sites					
	ρ_{I}		ρ_{II}		ρ_{III}	
	0.13		0.71		0.16	
	Mean/meV, standard deviation/meV					
Molecule	$E^{\mathrm{des}}_{\mathrm{mol,I}}$	$\sigma_{\mathrm{mol,I}}$	$E^{\mathrm{des}}_{\mathrm{mol,II}}$	$\sigma_{\mathrm{mol,II}}$	$E^{\mathrm{des}}_{\mathrm{mol,III}}$	$\sigma_{\mathrm{mol,III}}$
HD	30	3.3	40	4.3	55	4.5
D_2	30	3.3	42	4.3	58	4.5

The shift of the energy barriers from HD molecules to slightly higher values for D_2 molecules can be understood in light of their different atomic mass as discussed above. The fact that the leading edge of the 8 K curves is not reproduced well by the fit is probably due to the fact that the model does not include very shallow sites. Though one can add more site types to account for these features, this increases the computational cost and introduces additional fitting parameters, reducing the conclusiveness of our results. The essential properties of the surface can be captured by the three energies found here.

5.2 Irradiation with Atoms

TPD curves of tholin surfaces irradiated with H and D atoms (H+D) or D atoms (D+D) at several temperatures are presented in Figures 6 and 7, respectively. In these experiments atoms are deposited on the surface, where they diffuse and recombine. The resulting molecules stay on the surface—according to what is observed experimentally—and desorb later during the TPD. The only parameters that need to be fitted to these experiments are the energy barriers for diffusion and desorption of atoms, $E^{\mathrm{diff}}_{\mathrm{H}}$ and $E^{\mathrm{des}}_{\mathrm{H}}$.

The experiments presented here were performed at three different irradiation temperatures, 8 K, 12 K and 22 K. We observe that the desorption peaks of the 8 K experiments with atoms correspond to the desorption peaks of the experiments with molecules. Therefore, atoms have to become sufficiently mobile to form molecules already during the early stages of the TPD experiment. An acceptable fit of the TPD data is obtained only if the energy barrier for diffusion of atoms is at most $E_{\mathrm{H}}^{\mathrm{diff}} = 20$ meV. The corresponding energy barrier for desorption of atoms is then found as $E_{\mathrm{H}}^{\mathrm{des}} = 30$ meV.

As seen in Figures 6 and 7, the model correctly reproduces the general tendency of the traces to shift to higher temperatures if the irradiation temperature is increased. For irradiation at 12 K, however, it lags behind the experimental data by ≈ 3 K, and the predicted peak position still closely resembles the one found for irradiation with molecules. When atoms are irradiated at a surface temperature of 22 K, the fit is very good again.

Our comments at the end of Section 3 might suggest that the shift in TPD traces could be better reproduced by a model with several types of sites for atoms (corresponding to the types for molecules). Molecules produced on a certain type of site could then add specifically to this type's population, and their distribution (affected by atomic processes) might become more complex. We checked that such a model increases computational challenges, without improving the fits to experimental data.

6 Discussion

The formation of molecular hydrogen in space environments is of interest to several research fields: to astrophysicists studying star formation, since H_2 facilitates the cooling of a gravitationally collapsing cloud by absorbing UV light and re-radiating it in the IR (where the cloud is transparent); to astrochemists, because H_2 intervenes in most schemes of formation of other molecules in space; and to planetary scientists interested in the chemistry of atmospheres of bodies such as Titan. While the first experimental studies of H_2 formation were geared towards the measurement of the efficiency

of the reaction,[4] it was soon realized that one needed to understand the elementary steps of atom and molecule adsorption, diffusion on and desorption from heterogeneous surfaces. In the case of H interaction with tholins, experiments at higher temperatures imply that the formation of HD is governed by the abstraction of surface-bound H with D coming from the gas phase, and using IR spectroscopy it was noticed that incoming D atoms saturate some of the carbon-carbon, carbon-nitrogen, or nitrogen-nitrogen bonds of the tholin.[13] Our experiments of H and D interaction with tholin surfaces are performed at a lower temperature and show that the interaction is dominated by weak adsorption forces, and that the production of HD is consistent with the LH reaction mechanism. There are changes in the bonds of H and D with the surface, see Figure 10, due to partial saturation of C−H bonds with H and D atoms, but, if there is abstraction of H, this process is overwhelmed by the HD, H_2 and D_2 formation according to the processes described above. A detailed study of the changes of the IR features and IR and TPD results with samples at higher temperature will be presented elsewhere. In the meantime, we can only speculate on how our results and Sekine et al.'s[13] can be reconciled. Aside from possible differences in the reactivity of samples, it is possible

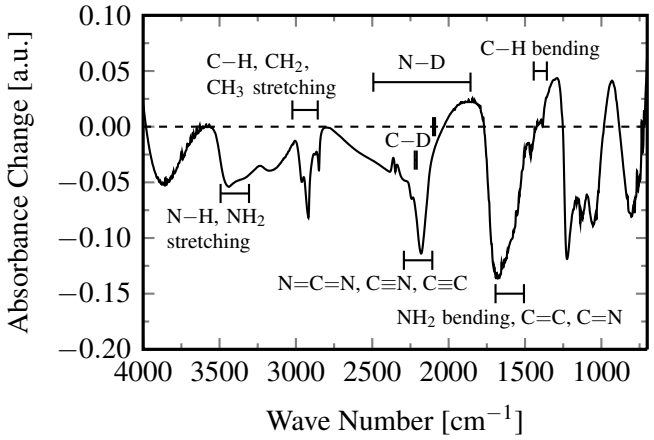

Figure 10: Change of infrared absorbance of the tholin sample after irradiation with H and D atoms for a cumulative dosage of 41 and 64 minutes, respectively. Increased absorption is above the horizontal line. Band assignments are indicated. The sample has been kept under vacuum for the whole duration of the experiments.

that thermal energy atoms striking the surface at low temperature experience the weak long-ranged physisorption interaction, while other channels become available at higher surface temperature. In

other words, H atoms might sample a precursor state. Examples of this behavior exist, such as H adsorption on Si.[45]

As an example of the application of our findings for the energy barriers of hydrogen on tholins, we show the implied results for the efficiency of H_2 formation on the surface of tholins in an environment resembling Titan's atmosphere. At a relevant height of about 700 km, we use a gas phase temperature of $T_{\mathrm{gas}} = 150$ K. The average thermal velocity of hydrogen atoms at this temperature is $v_{\mathrm{H}} = 1.8 \times 10^5$ cm/s, and we take a density of $\rho_{\mathrm{H}} = 5.9 \times 10^7$ cm^{-3} in the gas phase.[21] For the density $s = 5 \times 10^{14}$ sites/cm^2 assumed in Section 2.2 we obtain a flux per site $f = \rho_{\mathrm{H}} v_{\mathrm{H}}/(4s) = 5.3 \times 10^{-3}$ ML/s. The factor $1/4$ in the last relation results from the ratio between the (geometrical) cross section and the surface area of a sphere.

We calculate the efficiency $2D_{\mathrm{H}} n_{\mathrm{H}}^2/f$ using the analytic solution of the steady-state rate equation, Eq. (9a) with $\mathrm{d}n_{\mathrm{H}}/\mathrm{d}t \equiv 0$, which provides accurate results for sufficiently large grains. Figure 11 shows that a high efficiency window is found between 6 K and 15 K. At temperatures below that window, diffusion of atoms from one site to the other is so slow that they are nearly immobile, and therefore the LH kinetics largely prevents sticking of impinging atoms. On the other hand at temperatures higher than ≈ 15 K, the residence time of H atoms is very short, they do not encounter each other on the surface before they desorb, and the efficiency drops as well. For temperatures higher than this, other mechanisms might take over in which one of the partners is held on the surface by stronger adsorption forces. Preliminary analysis of data taken at higher sample temperature (> 30 K) shows that the HD formation rate is dramatically curtailed. The quantification of the formation of HD at these higher sample temperatures is ongoing.

7 Summary

We have studied the interaction of atomic and molecular hydrogen with tholin surfaces, using TPD experiments at low temperatures. Employing a fine-grained rate equation model to fit TPD traces, we have obtained energy barriers for the diffusion and desorption of both atomic as well as

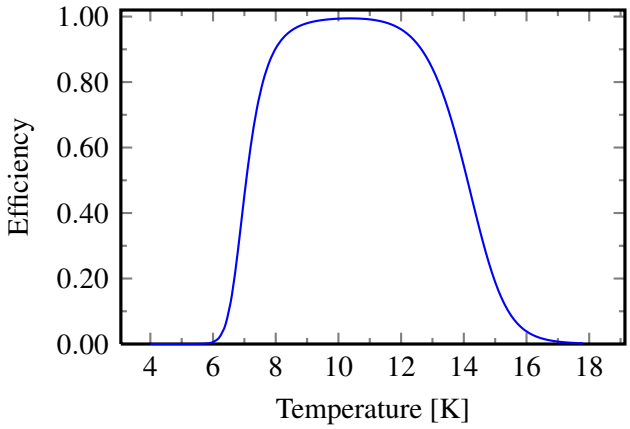

Figure 11: Efficiency of H_2 production on tholin as a function of the temperature for the surface parameters obtained in Section 5.2.

molecular hydrogen. The analysis shows that there are three types of sites for molecules, and each type is associated with a distribution of the energy barriers that can be fitted by a normal distribution. In contrast, there are no indications for a broad distribution of energy barriers for the atoms, and the data can be fitted using a single barrier. All barriers are below 60 meV, with the implication that the interactions with the surface are only governed by weak adsorption forces. The temperature window of efficient formation of molecular hydrogen depends on the diffusion and desorption barriers of the atoms, and not on the interaction of the molecules with the surface.

Acknowledgement

We are grateful to Prof. Mark Smith of the University of Arizona for providing the samples and to Dr. Imanaka (University of Arizona) for discussions. We thank the US-Israel Binational Science Foundation for support. G.V. was supported by NSF Grant AST-0507405.

References

(1) Schlapbach, L.; Züttel, A. *Nature* **2001**, *414*, 353–358.

(2) *Molecular Hydrogen in Space*; Combes, F., Pineau des Forets, G., Eds.; Cambridge University Press: Cambridge, 2000.

(3) Williams, D. A.; Brown, W. A.; Price, S. D.; Rawlings, J. M. C.; Viti, S. *Astron. & Geophys.* **2007**, *48*, 1.25–1.34.

(4) Pirronello, V.; Liu, C.; Shen, L.; Vidali, G. *Astrophys. J. Lett.* **1997**, *475*, L69–72.

(5) Perets, H. B.; Lederhendler, A.; Biham, O.; Vidali, G.; Li, L.; Swords, S.; Congiu, E.; Roser, J.; Manicò, G.; Brucato, J. R.; Pirronello, V. *Astrophys. J. Lett.* **2007**, *661*, L163–166.

(6) Vidali, G.; Li, L.; Roser, J. E.; Badman, R. *Adv. Space. Res.* **2009**, *43*, 1291–1298.

(7) Pirronello, V.; Liu, C.; Roser, J. E.; Vidali, G. *Astron. Astrophys.* **1999**, *344*, 681–686.

(8) Roser, J. E.; Swords, S.; Vidali, G. *Astrophys. J. Lett.* **2003**, *596*, L55–58.

(9) Hornekær, L.; Baurichter, A.; Petrunin, V. V.; Field, D.; Luntz, A. C. *Science* **2003**, *302*, 1943–1946.

(10) Amiaud, L.; Fillion, J. H.; Baouche, S.; Dulieu, F.; Momeni, A.; Lemaire, J. L. *J. Chem. Phys.* **2006**, *124*, 094702.

(11) Langmuir, I. *J. Am. Chem. Soc.* **1918**, *40*, 1361–1403.

(12) Mennella, V. *Astrophys. J. Lett.* **2008**, *684*, L25–28.

(13) Sekine, Y.; Imanaka, H.; Matsui, T.; Khare, B. N.; Bakes, E. L. O.; McKay, C. P.; Sugita, S. *Icarus* **2008**, *194*, 186–200.

(14) McKay, C. P.; Coustenis, A.; Samuelson, R. E.; Lemmon, M. T.; Lorenz, R. D.; Cabane, M.; Rannou, P.; Drossart, P. *Planet. and Space Sci.* **2001**, *49*, 79–99.

(15) Szopa, C.; Cernogora, G.; Boufendi, L.; Correia, J. J.; Coll, P. *Planetary and Space Science* **2006**, *54*, 394–404.

(16) Khare, B. N.; Sagan, C.; Thompson, W. R.; Arakawa, E. T.; Suits, F.; Callcott, T. A.; Williams, M. W.; Shrader, S.; Ogino, H.; Willingham, T. O.; Nagy, B. *Advances in Space Research* **1984**, *4*, 59–68.

(17) Sagan, S.; Khare, B. N. *Nature* **1979**, *277*, 102–107.

(18) Coll, P.; Coscia, D.; Smith, N.; Gazeau, M.-C.; Ramírez, S. I.; Cernogora, G.; Israël, G.; Raulin, F. *Planet. and Space Sci.* **1999**, *47*, 1331–1340.

(19) Imanaka, H.; Khare, B. N.; Elsila, J. E.; Bakes, E. L. O.; McKay, C. P.; Cruikshank, D. P.; Sugita, S.; Matsui, T.; Zare, R. N. *Icarus* **2004**, *168*, 344–366.

(20) Quirico, E.; Montagnac, G.; Lees, V.; McMillan, P. F.; Szopa, C.; Cernogora, G.; Rouzaud, J.-N.; Simon, P.; Bernard, J.-M.; Coll, P.; Fray, N.; Minard, R. D.; Raulin, F.; Reynard, B.; Schmitt, B. *Icarus* **2008**, *198*, 218–231.

(21) Lebonnois, S.; Bakes, E. L. O.; McKay, C. P. *Icarus* **2003**, *161*, 474–485.

(22) Young, Y. L.; Allen, M.; Pinto, J. P. *Astrophys. J. Suppl.* **1984**, *55*, 465.

(23) Duley, W. W.; Williams, D. A. *Interstellar Chemistry*; Academic Press, 1984.

(24) Bakes, E. L. O.; Lebonnois, S.; Bauschlicher, C. W., Jr.; McKay, C. P. *Icarus* **2003**, *161*, 468–473.

(25) Duley, W. W. *Mon. Not. Roy. Astron. Soc.* **1996**, *279*, 591–594.

(26) Harris, J.; Kasemo, B. *Surf. Sci.* **1981**, *105*, L281–287.

(27) Rettner, C. T. *J. Chem. Phys.* **1994**, *101*, 1529–1546.

(28) Eilmsteiner, G.; Walkner, W.; Winkler, A. *Surf. Sci.* **1996**, *352–354*, 263–267.

(29) Khan, A. R.; Takeo, A.; Ueno, S.; Inanaga, S.; Yamauchi, T.; Narita, Y.; Tsurumaki, H.; Namiki, A. *Surf. Sci.* **2007**, *601*, 1635–1641.

(30) Zecho, T.; Güttler, A.; Sha, X.; Jackson, B.; Küppers, J. *J. Chem. Phys.* **2002**, *117*, 8486.

(31) Vidali, G.; Pirronello, V.; Li, L.; Roser, J.; Manicó, G.; Congiu, E.; Mehl, H.; Lederhendler, A.; Perets, H. B.; Brucato, J. R.; Biham, O. *J. Phys. Chem. A* **2007**, *111*, 12611–12619.

(32) Katz, N.; Furman, I.; Biham, O.; Pirronello, V.; Vidali, G. *Astrophys. J.* **1999**, *522*, 305–312.

(33) Manicò, G.; Ragunì, G.; Pirronello, V.; Roser, J. E.; Vidali, G. *Astrophys. J. Lett.* **2001**, *548*, L253–256.

(34) Perets, H. B.; Biham, O.; Manicó, G.; Pirronello, V.; Roser, J.; Swords, S.; Vidali, G. *Astrophys. J.* **2005**, *627*, 850–860.

(35) Vidali, G.; Roser, J.; Manicó, G.; Pirronello, V.; Perets, H. B.; Biham, O. *J. Phys.: Conf. Ser.* **2005**, *6*, 36–58.

(36) Neish, C. D.; Somogyi, Á.; Smith, M. A. *Astrobiol.* **2010**, *10*, 337–347.

(37) Neish, C. D.; Somogyi, Á.; Lunine, J. I.; Smith, M. A. *Icarus* **2009**, *201*, 412–421.

(38) Sarker, N.; Somogyi, A.; Lunine, J. I.; Smith, M. A. *Astrobiol.* **2003**, *3*, 719–726.

(39) Yates, J. T. In *Methods of Experimental Physics, Solid State Physics: Surfaces*; Academic Press: New York, 1985; Vol. 22, p 425.

(40) Barton, S. S.; Harrison, B. H.; Dollimore, J. *J. Phys. Chem.* **1978**, *82*, 290–294.

(41) Cazaux, S.; Tielens, A. G. G. M. *Astrophys. J.* **2004**, *604*, 222–237.

(42) Barrie, P. J. *Phys. Chem. Chem. Phys.* **2008**, *10*, 1688–1696.

(43) Vidali, G.; Li, L. *J. Phys.: Condens. Matter* **2010**, *22*, 304012.

(44) Ghio, E.; Mattera, L.; Salvo, C.; Tommasini, F.; Valbusa, U. *J. Chem. Phys.* **1980**, *73*, 556–561.

(45) Tok, E. S.; Engstrom, J. R.; Kang, H. C. *J. Chem. Phys.* **2003**, *118*, 3294–3299.